β-arrestin–dependent PI(4,5)P_2 synthesis boosts GPCR endocytosis

Seung-Ryoung Jung[a,b,c,1], Yifei Jiang[b], Jong Bae Seo[d,e], Daniel T. Chiu[b,f], Bertil Hille[a], and Duk-Su Koh[a]

[a]Department of Physiology and Biophysics, University of Washington, Seattle, WA 98195; [b]Department of Chemistry, University of Washington, Seattle, WA 98195; [c]Department of Biomedical Engineering, Southern University of Science and Technology, Shenzhen, Guangdong 518055, China; [d]Department of Biosciences, Mokpo National University, Jeonnam 58554, Republic of Korea; [e]Department of Biomedicine, Health and Life Convergence Sciences, Mokpo National University, Jeonnam 58554, Republic of Korea; and [f]Department of Bioengineering, University of Washington, Seattle, WA 98195

Edited by Pietro De Camilli, Yale University and HHMI, New Haven, CT, and approved March 19, 2021 (received for review May 29, 2020)

β-arrestins regulate many cellular functions including intracellular signaling and desensitization of G protein–coupled receptors (GPCRs). Previous studies show that β-arrestin signaling and receptor endocytosis are modulated by the plasma membrane phosphoinositide lipid phosphatidylinositol-(4, 5)-bisphosphate (PI(4,5)P_2). We found that β-arrestin also helped promote synthesis of PI(4,5)P_2 and up-regulated GPCR endocytosis. We studied these questions with the G_q-coupled protease-activated receptor 2 (PAR2), which activates phospholipase C, desensitizes quickly, and undergoes extensive endocytosis. Phosphoinositides were monitored and controlled in live cells using lipid-specific fluorescent probes and genetic tools. Applying PAR2 agonist initiated depletion of PI(4,5)P_2, which then recovered during rapid receptor desensitization, giving way to endocytosis. This endocytosis could be reduced by various manipulations that depleted phosphoinositides again right after phosphoinositide recovery: PI(4)P, a precusor of PI(4,5)P_2, could be depleted at either the Golgi or the plasma membrane (PM) using a recruitable lipid 4-phosphatase enzyme and PI(4,5)P_2 could be depleted at the PM using a recruitable 5-phosphatase. Endocytosis required the phosphoinositides. Knock-down of β-arrestin revealed that endogenous β-arrestin normally doubles the rate of PIP5-kinase (PIP5K) after PAR2 desensitization, boosting PI(4,5)P_2-dependent formation of clathrin-coated pits (CCPs) at the PM. Desensitized PAR2 receptors were swiftly immobilized when they encountered CCPs, showing a dwell time of ∼90 s, 100 times longer than for unactivated receptors. PAR2/β-arrestin complexes eventually accumulated around the edges or across the surface of CCPs promoting transient binding of PIP5K-Iγ. Taken together, β-arrestins can coordinate potentiation of PIP5K activity at CCPs to induce local PI(4,5)P_2 generation that promotes recruitment of PI(4,5)P_2-dependent endocytic machinery.

β | phosphoinositide lipids | GPCR | endocytosis | PIP5K

Membrane phosphatidylinositide lipids (PPIs) are dynamic regulators of diverse cell functions, and their dysregulation underlies numerous human diseases (1). This paper concerns the key involvement of plasma membrane (PM) phosphatidylinositol-(4, 5)-bisphosphate (PI(4,5)P_2) in refining receptor–G protein and receptor–β-arrestin coupling (2, 3) and preparing for the endocytosis of receptors (4). Endocytosis requires clustering of adapter proteins on the PM, nucleation of clathrin-coated membrane pits, capture of receptors with β-arrestin (5–7), and pinching off of pits as intracellular vesicles by dynamin GTPase (4, 8–10). In clathrin-mediated endocytosis, PI(4,5)P_2 is typically needed for the assembly of the adaptor protein complexes, clathrin-coated pits (CCPs), and dynamin complexes (4, 11–14). Hence, receptor internalization should be compromised if PI(4,5)P_2 pools are depleted. This raises the question of how receptors that signal by depleting PI(4,5)P_2 can still be internalized. In this study, we found roles of receptor stimulation and β-arrestin in promoting resynthesis of PI(4,5)P_2, thus enabling endocytosis at the PM.

Synthesis of PPIs starts with phosphatidylinositol and families of lipid kinases that generate the mono-, bis-, and tris-phosphorylated inositol ring. PM phosphatidylinositol 4-phosphate (PI(4)P) and PI(4,5)P_2 are produced by several mechanisms potentially involving other membrane compartments. They can be synthesized by lipid 4-kinases acting on PM phosphatidylinositol and by lipid 5-kinases acting on PM PI(4)P; they can be delivered in exchange for other lipids by phosphatidylinositol exchange proteins; and they can be delivered through fusion with other membranes (15–23). Such studies show that the PPI pools in different membranes are interdependent (21). For example, depleting PI(4)P locally in the *trans*-Golgi using a recruitable PI(4)P 4-phosphatase tool reduces the generation of PI(4,5)P_2 at the PM (24). Conversely, depleting PI(4,5)P_2 at the PM by activating muscarinic or angiotensin II receptors also strongly decreases total cellular PI(4)P (25–27). New evidence is emerging that the PPI composition controls membrane trafficking between organelles. For instance, trafficking of mannose 6-phosphate receptors from the Golgi to the PM can be slowed by reduction of PPI synthesis (28) presumably because PPIs are important for fusion of receptor-containing vesicles with the PM.

Here, we study contributions of PPI pools to the endocytosis of the G_q-coupled protease-activated receptor 2 (PAR2). This receptor is involved in inflammatory responses (29), sensation of inflammatory pain (30), and cancer metastasis (31). It has been a target of drug development (32) facilitated by recent crystal structures (33). Stimulation of this receptor activates phospholipase C (PLC) to cleave and deplete PI(4,5)P_2 with accompanying production of diacylglycerol, inositol trisphosphate, and calcium signals (34, 35). Activation of the PAR-receptor family has unique properties. The receptor is activated by cleavage of the N terminus

Significance

Stimulation of protease-activated receptor 2 (PAR2) at the plasma membrane triggers a branching cascade of interrelated events in several cellular compartments. In one branch, the G protein G_q couples to phospholipase C, and the membrane phosphoinositide lipids PI(4,5)P_2 and PI(4)P are depleted. In another branch, the receptor becomes desensitized by becoming phosphorylated, bound to β-arrestin, and internalized by clathrin-coated pits. This second branch needs PI(4,5)P_2 at several steps. We found that β-arrestin in complex with receptors stably binds to clathrin-coated pits and increases transient binding of the PI(4,5)P_2 synthetic enzyme PIP5K-Iγ. Then, this complex in clathrin-coated pits boosts the rate of PI(4,5)P_2 synthesis from Golgi and plasma membrane PI(4)P, so that PI(4,5)P_2 becomes elevated. The new PI(4,5)P_2 allows receptor internalization.

Author contributions: S.-R.J., B.H., and D.-S.K. designed research; S.-R.J. performed research; S.-R.J., Y.J., J.B.S., D.T.C., B.H., and D.-S.K. contributed new reagents/analytic tools; S.-R.J. analyzed data; S.-R.J., B.H., and D.-S.K. wrote the paper; and S.-R.J. supervised the project.

The authors declare no competing interest.

This article is a PNAS Direct Submission.

[1]To whom correspondence may be addressed. Email: jsr007@uw.edu.

This article contains supporting information online at https://www.pnas.org/lookup/suppl/doi:10.1073/pnas.2011023118/-/DCSupplemental.

Published April 20, 2021.

by serine proteases such as thrombin, tryptase, or trypsin (34, 36), which generates a tethered N-terminal ligand. The activation stimulates G_q but is followed quickly by desensitization that terminates G_q signaling (34, 35, 37). Our previous experimental results and mathematical modeling suggest that rapid phosphorylation of PAR2 precedes desensitization and that β-arrrestin clamps the phosphorylated and ligand-bound state of the receptor, protecting it from dephosphorylation by serine/threonine phosphatases (38). Then, the receptor is internalized slowly via a clathrin- and dynamin-dependent pathway (8). This rapidly desensitizing receptor is well suited to address mechanisms involved in PPI lipid–dependent G_qPCR endocytosis.

Using genetic and optical tools to manipulate and measure PI(4)P and PI(4,5)P_2 levels acutely at the Golgi or the PM, we now demonstrate that PAR2 internalization can be controlled by PM PI(4,5)P_2 that is replenished using both PM and Golgi pools of PI(4)P. A β-arrestin–dependent activation of PIP5-kinase (PIP5K) at the PM turned out to be critical in the formation of PI(4,5)P_2- and PI(4)P-requiring CCPs and potentially other endocytic machinery for receptor internalization.

Results

PI(4)P and PI(4,5)P_2 Pools Are Coupled. We started by monitoring changes of PI(4,5)P_2 and PI(4)P pools while the G_q-coupled PAR2 receptor was being activated. The receptor was transiently expressed and stimulated by applying a short activating peptide (AP) made of six amino acids (SLIGKT), which mimics the N-terminal tethered ligand sequence of cleaved receptors (35, 37, 38). PI(4,5)P_2 was monitored using a red fluorescent protein (RFP)-tagged pleckstrin homology (PH) domain of PLCδ1 (PH-RFP), and PI(4)P was monitored using a GFP-tagged P4M probe (GFP-P4M) (22, 39, 40). In resting cells, the expressed PH-RFP probe was localized to the PM (Fig. 1*A*, 108 s). Activation of PAR2-initiated depletion of PM PI(4,5)P_2, indicated by translocation of the PH-RFP probe from the PM to the cytoplasm (Fig. 1*A*, 132 s). Translocation was rapid (Fig. 1*B*, magenta trace), reflecting brisk initial hydrolysis of PM PI(4,5)P_2 by PLC. However, already within minutes, the probe had returned from the cytoplasm back to the PM even in the continuous presence of the PAR2 agonist, indicating that the receptors had desensitized, PLC had turned off, and PM PI(4,5)P_2 was replenished. In resting cells, the GFP-P4M probe marking PI(4)P localized to the Golgi and the PM (Fig. 1*A*, 108 s) as demonstrated previously (24, 40). Like for PI(4,5)P_2, activation of PAR2-initiated depletion of PI(4)P as indicated by translocation of GFP-P4M to the cytoplasm (Fig. 1*B*, green trace). Again within minutes, the released PI(4)P probe returned from the cytoplasm to both the PM (*SI Appendix*, Fig. S1) and the Golgi (Fig. 1*A* at 360 s). The time to half return of the PI(4)P probe to the PM was 87 ± 14 s, a little longer than the

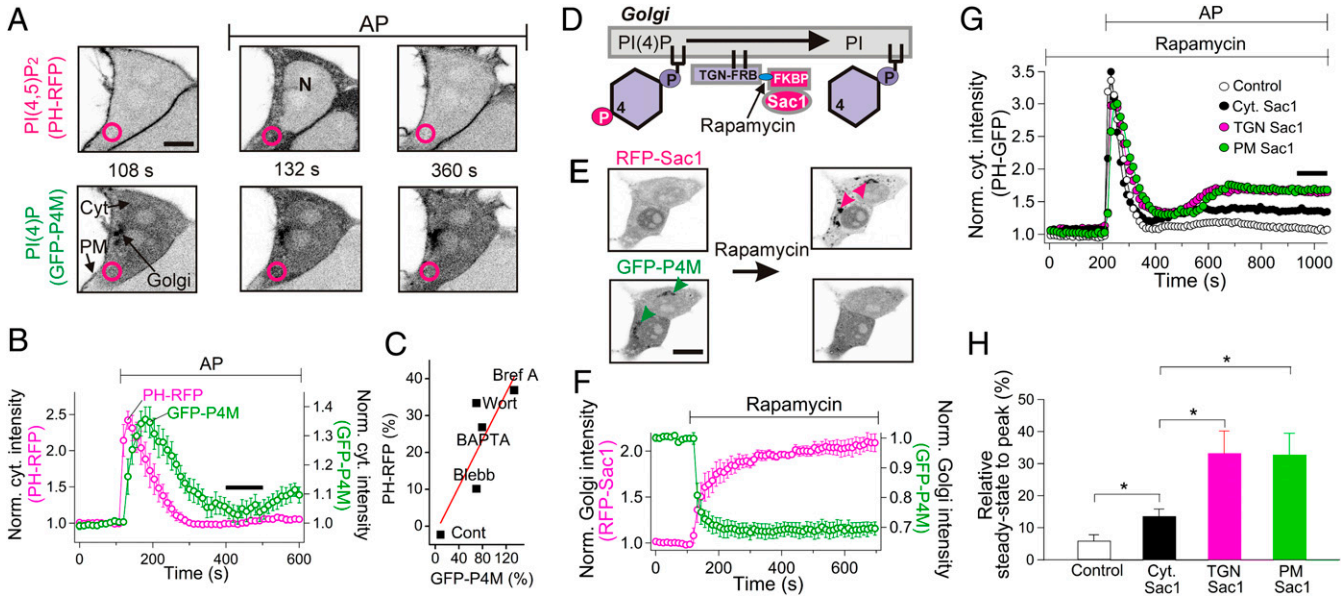

Fig. 1. PI(4)P and PI(4,5)P_2 pools are coupled. (*A*) Confocal images showing dynamic redistribution of the GFP-P4M probe reporting PI(4)P and the PH-RFP probe reporting PI(4,5)P_2, upon application of 100 μM AP to activate PAR2. The images have inverted contrast with fluorescence shown dark. Magenta circles indicate regions of interest chosen for measurements of cytoplasmic intensities with each probe. The labels denote the PM, Golgi, cytoplasm (Cyt), and nucleus (N). (Scale bar, 5 μm.) (*B*) Time courses of cytoplasmic intensities of PI(4)P and PI(4,5)P_2 probes during AP application. The intensities were normalized to reduce cell-to-cell variation and then averaged (Norm. cyt. intensity). PI(4,5)P_2 (magenta) and PI(4)P (green) ($n = 8$ cells). The recovery time constants were 58 ± 9 s (PH-RFP) and 89 ± 18 s (GFP-P4M). $P = 0.12$ (Student's paired t test). (*C*) Correlation of PI(4,5)P_2 and PI(4)P changes induced by different pharmacological perturbations. Signal amplitude (%) for each condition is calculated from the steady-state level (at 300 to 400 s after application of AP as indicated with a heavy bar in *B*) minus the initial baseline. Pearson's correlation coefficient for the linear fit (red line) was 0.85. Cells were pretreated with different drugs for 5 or 10 min before AP (*SI Appendix*, Fig. S2): Wortmannin (30 μM, $n = 6$ cells, Wort) and BAPTA-AM (50 μM, $n = 6$ cells, BAPTA), blebbistatin (30 μM, $n = 11$ cells, Blebb) and brefeldin A (10 μg/mL, $n = 4$ cells, Bref A). (*D*) A schematic of dephosphorylation of PI(4)P at the *trans*-Golgi using recruitable human Sac1 (Sac1) and rapamycin. (*E*) Inverted confocal images. Rapamycin (5 μM) induces translocation of RFP-Sac1-FKBP to the TGN38-FRB-CFP anchor at the *trans*-Golgi membrane (upper images, magenta arrow heads), and the Golgi-localized GFP-P4M probe (lower images, green arrow heads) is released to the cytoplasm. (Scale bar, 10 μm.) (*F*) Time courses of Golgi Sac1 (magenta) and the GFP-P4M probe (green) following rapamycin application. Intensities are normalized to the control values before rapamycin and averaged ($n = 5$ cells). (*G*) Time course of cytoplasmic PH-GFP showing the effect of PI(4)P depletion at the Golgi and the PM on the recovery of PM PI(4,5P)$_2$ following PAR2 desensitization. Cells were pretreated with rapamycin for 10 min before the application of 100 μM AP. The figure shows only 3 min rapamycin treatment prior to the AP treatment. Plotted are control cells (Control), cells expressing cytoplasmic Sac1 alone without TGN38-FRB-CFP or LDR-CFP (Cyt. Sac1), and cells where Sac1 is recruited to either the *trans*-Golgi (TGN Sac1) or the PM (PM Sac1). (*H*) Analysis of cytoplasmic PH-GFP responses, summarizing the secondary depletion of PI(4,5)P_2 without or with Sac1 recruitment to the Golgi or the PM. Mean values obtained from the time window between 950 and 1,050 s (black bar in *G*) were compared to the peak to get the relative steady state. The values in G and H are averages. Control ($n = 8$ cells), Sac1 alone ($n = 9$ cells), TGN Sac1 ($n = 7$ cells), and PM Sac1 ($n = 6$ cells). *$P < 0.05$.

half return of the PI(4,5)P_2 probe, 54 ± 3.4 s (*SI Appendix*, Fig. S1). The recovery and resynthesis of phosphoinositide pools is a special focus of this paper.

The PI(4)P and PI(4,5)P_2 pools are coupled by metabolism and by transport mechanisms. When PI4-kinase, the enzyme that synthesizes PI(4)P, was inhibited with wortmannin or when trafficking of intracellular PI(4)P from the Golgi to the PM was compromised by brefeldin A or BAPTA-AM treatment, the recovery of the PI(4)P and PI(4,5)P_2 pools became incomplete (*SI Appendix*, Fig. S2 and *Supplementary Discussion*). We compared the extent of recovery of the two phosphoinositides after PAR2-mediated hydrolysis of PI(4,5)P_2 (during the black bar in Fig. 1*B*). The less complete the PI(4)P recovery was, the less complete the recovery of PI(4,5)P_2 (Fig. 1*C*, Pearson's correlation coefficient, 0.85), reflecting the dynamic linkage of these lipid pools.

We selectively manipulated the two local PI(4)P pools enzymatically to assess whether they both served as major sources for resynthesis of PM PI(4,5)P_2 after PAR2 activation. The strategy was to use induced chemical dimerization to recruit a lipid phosphatase to an appropriate cell membrane (41). An FKBP-tagged, genetically engineered lipid 4-phosphatase human Sac1 ("Sac1-FKBP") enzyme was recruited to FKBP-rapamycin binding (FRB) domain-tagged membrane anchors using rapamycin (Fig. 1*D*). While not a perfectly selective 4-phosphatase, this enzyme has a substrate preference for PI(4)P that is 3 times higher than for PI(3)P and 10 times higher than for other phosphoinositide substrates (42). The PI(4)P of the Golgi or the PM was depleted by recruiting Sac1-FKBP from the cytoplasm to two different compartmental membrane anchors: TGN38-CFP (cyan fluorescent protein) fused with FRB (TGN-FRB) for *trans*-Golgi targeting and LDR-CFP for PM targeting (24). When RFP-tagged Sac1-FKBP was translocated to the *trans*-Golgi network, the P4M probe was released from the Golgi, indicating depletion of Golgi PI(4)P (Fig. 1*E*). The probe was released (exponential time constant $\tau = 16 \pm 5$ s, $n = 5$, Fig. 1*F*, green symbols) well before Sac1 translocation was completed ($\tau = 77 \pm 32$ s, $n = 5$, magenta symbols), showing that only a small fraction of the translocatable Sac1 enzyme sufficed to deplete the Golgi PI(4)P. We then asked how prior depletion of PI(4)P affected PM PI(4,5)P_2 recovery during AP treatment (Fig. 1 *G* and *H*). In control cells without overexpressed Sac1, PM PI(4,5)P_2 recovery during AP was nearly complete, leaving only a small residual steady-state level of cytoplasmic PH probe (6 ± 2.4%, $n = 8$, Fig. 1 *G* and *H*, black open symbol and bar, respectively) compared to the maximum peak level during AP treatment. With the Sac1 construct alone without membrane anchors, the residual steady state during AP was slightly higher (14 ± 2.4%, $n = 9$, $P = 0.02$, Fig. 1 *G* and *H*, black filled symbols and bar). Perhaps the untargeted cytoplasmic Sac1 partially depleted PI(4)P and thus compromised full PI(4,5)P_2 recovery at the PM (40). In the cells with Sac1 recruited by rapamyin to the Golgi anchor TGN38, the cytoplasmic residual steady-state PH probe after AP was greater, 33 ± 7% ($n = 7$, $P = 0.047$, Fig. 1 *G* and *H*, magenta symbols and bar). To validate the specificity of the Golgi anchor, Sac1 was also recruited to a different Golgi-anchoring protein, giantin-FRB, giving results similar to those with TGN-FRB (*SI Appendix*, Fig. S3). Finally, Sac1 was recruited to the PM anchor LDR-CFP, which affected PM PI(4,5)P_2 recovery to the same extent as with the two Golgi anchors (33 ± 7%, $n = 6$, $P = 0.02$, Fig. 1 *G* and *H*, green symbols and bar). In conclusion, two pools of PI(4)P, one at the Golgi and the other at the PM, contribute significantly to the restoration of PM PI(4,5)P_2 after PAR2 desensitization.

PI(4)P and PI(4,5)P_2 Support the Internalization of PAR2. We next looked for roles of phosphoinositides in PAR2 internalization. We previously reported rapid kinetics of formation of complexes between β-arrestin and activated PAR2 that govern receptor desensitization (38). Such complexes can become localized to CCPs (8). At least eight of the proteins involved in receptor internalization, including β-arrestin, adaptor proteins, and dynamin, interact with PI(4,5)P_2 (4). Therefore, we expected that PAR2 internalization from the PM could be compromised by depleting PM PI(4,5)P_2 (43) or its precursor PI(4)P. The internalization of PAR2 was imaged with an Alexa647 dye–labeled primary antibody against an extracellular epitope of PAR2 (*SI Appendix*, Fig. S4, ref. 43). Using the recruitable Sac1 system to deplete PI(4)P pools at the Golgi or the PM, significantly reduced AP-induced internalization of PAR2 receptors compared to control experiments with AP alone (net reduction of internalization was 50% for Golgi depletion and 54% for PM, Fig. 2 *A* and *B*). As negative controls, without recruitable Sac1 rapamycin neither initiated large PAR2 internalization without AP (Fig. 2 *A* and *B*) nor reduced internalization induced by AP (*SI Appendix*, Fig. S5). Next, we instead depleted PM PI(4,5)P_2 using a translocatable lipid 5-phosphatase [Fig. 2*C* (24, 41)]. Adding rapamycin raised the cytoplasmic intensity of the PH probe to ~40% of the earlier peak level induced by AP (Fig. 2*D*), confirming a partial depletion of PM PI(4,5)P_2. In parallel, PAR2 internalization was significantly reduced (by 81%), consistent with the hypothesis that PM PI(4,5)P_2 is essential for endocytosis of PAR2 (Fig. 2*E*).

β-Arrestin Boosts PI(4,5)P_2 Synthesis at the PM. Does regulation of PAR2 endocytosis by phosphoinositide lipids (PPIs) involve β-arrestin? Already we know that the β-arrestins have a PPI binding site (44), and a cryogenic electron microscopy (cryo-EM) structure shows that PI(4,5)P_2 can be stably incorporated into a complex of β-arrestin with neurotensin receptors (3). In our experiments, β-arrestin 2 translocated to the PM upon PAR2 activation (Fig. 3*A*, at 286 s) and then relocated to intracellular puncta during internalization of receptors (Fig. 3*A*, at 396 and 1,028 s). Our fluorescence resonance energy transfer (FRET) assay reported interactions closer than 10 nm between β-arrestin-2-YFP (yellow fluorescent protein) and PAR2-CFP molecules, increasing gradually and robustly over a 5 min period during continued AP application (Fig. 3*B*). We interpret the FRET increase as formation of molecular complexes between β-arrestin 2 and PAR2 receptors. We tested blockers of receptor kinases: 30 μM compound101 (cmpd101) blocking GRK2/3 and 100 nM bisindolylmaleimide1 (BIS1) blocking protein kinase C. Together, they significantly reduced development of the FRET interaction (Fig. 3*B*). Hence, as anticipated, receptor phosphorylation facilitates formation of β-arrestin 2-PAR2 complexes.

The β-arrestin translocation to the PM also was retarded by making mutations in the PI(4,5)P_2 binding site on β-arrestin as defined in cryo-EM and cell biological studies (3, 44). To ask whether acute depletion of PI(4,5)P_2 can also slow β-arrestin translocation, the PI(4,5)P_2 5-phosphatase was recruited to the PM anchor by applying rapamycin shortly after partial depletion of PI(4,5)P_2 by activated PAR2. The recruited 5-phosphatase further depleted PM PI(4,5)P_2 compared to control (Fig. 3*C*). The phosphatase also slowed the recovery of PI(4,5)P_2 (control time constant 79 ± 12 s for AP alone [$n = 6$] versus 242 ± 60 s for 5-phosphatase [$n = 8$], $P = 0.04$) and made the recovery incomplete. Further, the translocation of β-arrestin 2 was significantly delayed by this protracted PI(4,5)P_2 depletion (half maximal time for translocation was 49 ± 4 s in control [$n = 8$] versus 79 ± 7 s with 5-phosphatase [$n = 6$], $P = 0.007$, Fig. 3 *D*, *Inset*). Nevertheless, the extent of final translocation was unchanged (0.33 ± 0.05 for control versus 0.33 ± 0.02 with 5-phosphatase, $P = 0.96$, Fig. 3*D*; ref. 45). Hence, the initial association of β-arrestin 2 with PAR2 seems accelerated by PI(4,5)P_2, consistent with structural and in vitro observations (3).

We recognized a correlation between the rate of synthesis of PM PI(4,5)P_2 and the presence of β-arrestin. In the first experiment, PI(4,5)P_2 was partially depleted by translocating 5-phosphatase to the PM with rapamycin (Fig. 3*E*, without small interfering RNA [siRNA]). Then, PAR2 receptors were activated with AP to stimulate PLC. The PM PI(4,5)P_2 became depleted further, and then

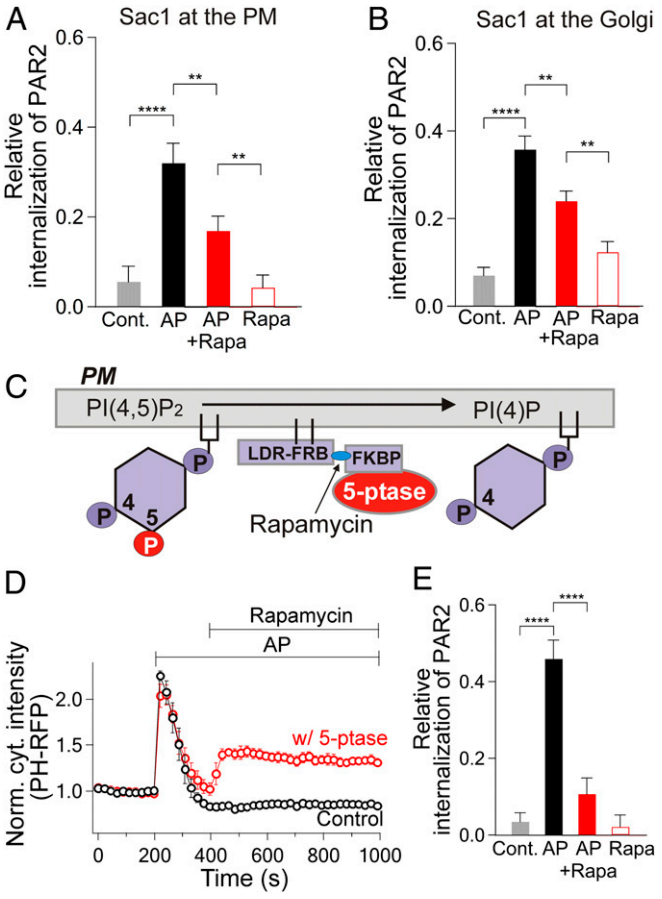

Fig. 2. PI(4)P and PI(4,5)P_2 support the internalization of PAR2. (*A* and *B*) Relative internalization of PAR2 estimated from the ratio of cytoplasmic PAR2 to the total PAR2 (*SI Appendix, Methods and Materials* and Fig. S4). Cells were untreated (Cont.) or incubated with 100 μM AP for 1 h (AP). For the rapamycin group, cells were treated with 5 μM rapamycin (Rapa) or with AP and rapamycin (AP+Rapa), which would recruit Sac1 4-phosphatase to the PM (*A*) or to the *trans*-Golgi (*B*). Each condition is an average of 7 to 17 cells from two independent experiments. (*C*) A schematic diagram of 5-phosphatase tagged with FKBP (5-ptase-FKBP) being recruited to PM-linked LDR-FRB-CFP (LDR-FRB). (*D*) Normalized time course of cytoplasmic intensity of PH-RFP probe during application of AP. Rapamycin (5 μM) was added after full recovery of the PH-RFP probe (w/5-ptase, $n = 7$ cells). The black symbols indicate the control experiment without 5-phosphatase overexpression (control, $n = 5$ cells). (*E*) Average of PAR2 internalization in the absence or presence of 5-phosphatase from 9 to 16 cells for each condition. $^{**}P < 0.01$; $^{****}P < 0.001$.

as the receptors desensitized, PI(4,5)P_2 began to recover. Unexpectedly, the PI(4,5)P_2 recovery was strong enough to surpass the previous level from before AP addition (Fig. 3*E*, without siRNA), as if PAR2 activation had accelerated the lipid kinases that restore PI(4,5)P_2. Could this acceleration be due to a recruitment of β-arrestins? Indeed, the acceleration was significantly diminished by knocking down β-arrestin 1 and 2 using siRNA compared to control siRNA (40% decrease of β-arrestin 1 and 2 protein level) (38) (Fig. 3 *E* and *F*). Furthermore, inhibitors of β-arrestin recruitment (compound101/BIS1) led to secondary PI(4,5)P_2 depletion (Fig. 3*G*). Apparently, lipid kinases are accelerated during PAR2 desensitization by a process that involves β-arrestins.

PAR2 Stimulation Activates PIP5K. A potentiation of endogenous PIP5K activity after activation of PAR2 was readily observed. Our strategy was to dephosphorylate PI(4,5)P_2 to PI(4)P rapidly with a voltage-sensitive 5-phosphatase (Dr-VSP) and then to measure the rate of rephosphorylation to PI(4,5)P_2 using the PH-RFP probe (Fig. 4 *A–D*). When Dr-VSP was activated by a voltage jump to +100 mV for 2 s under whole-cell patch clamp, the PH probe translocated to the cytoplasm, and after the voltage pulse, the probe returned to the PM within 10 to 15 s (Fig. 4*D*). An exponential fit to this return measured the rate constant for endogenous PIP5K activity. In control, the time constant was ∼10 s, and therefore the rate constant was 0.10/s. The next experiment evoked transient migration of PH probes by application of PAR2 receptor agonist AP (Fig. 4*E*, black symbols). Assaying with the VSP protocol before and periodically after this agonist treatment showed that the 5-kinase activity was increased approximately twofold ($P = 0.01$) by AP and sustained this level for >6 min (Fig. 4*E*, red symbols). As a control, we verified that the translocation of the PH-RFP probe was not sensitive to the level of cytoplasmic IP_3 without PAR2 activation. Specifically, including 50 μM IP_3 in the whole-cell patch pipette did not promote translocation of the PH-RFP probe into the cytoplasmic compartment and did not change the recovery rate constant of the PH probe after VSP activation (0.11 ± 0.02/s in control [$n = 3$] versus 0.11 ± 0.01/s with IP_3 [$n = 5$], $P = 0.69$). To be more precise, the test with Dr-VSP measures the catalytic rate constant of the PIP5K reaction at the PM by transiently creating an artificial pool of PI(4)P at the PM. Without VSP, the rate of production of PI(4,5)P_2 at any moment would be given by this rate constant multiplied by the endogenous local PI(4)P pool size.

In subsequent experiments, we observed that the spatial distribution of an overexpressed 5-kinase became reorganized to clusters of β-arrestin 2. Using conventional total-internal reflection fluorescence (TIRF) microscopy, we identified nascent clusters of β-arrestin 2 growing over 5 to 10 min during AP action (Fig. 4*F*, magenta, and *SI Appendix*, Fig. S6). About 50% of the clusters (group 1, Fig. 4*F*, green) showed a parallel growing recruitment of the overexpressed human GFP-phosphatidylinositol-4-phosphate 5-kinase (full-length type-1 gamma p87 [PIP5K-Iγ]). The other 50% of the arrestin clusters (group 2, Fig. 4*G*, green), showed an initial fall of 5-kinase followed by a later growing accumulation. In this second group, the clustering of β-arrestin 2 proceeded slightly more slowly compared to the group 1 case (gray trace replotted from the magenta trace in Fig. 4*F*, $P < 0.0001$), again as if clustering of PIP5K-Iγ and β-arrestins were interdependent. As another test for an interaction between PIP5K-Iγ and β-arrestins, we designed a FRET experiment with a PIP5K-Iγ construct that was engineered to be localized in the cytoplasm at rest (41). The FRET assay revealed a rapidly developing physical proximity between the engineered CFP-PIP5K-Iγ and β-arrestin-2-YFP during PAR2 activation (Fig. 4*H*).

We next examined whether mutations of a PPI binding site identified in β-arrestin could reduce PI(4,5)P_2 regeneration and PAR2 endocytosis since PI(4,5)P_2 binding might play a key role for recruiting PIP5K (Fig. 5*A*, 46). Two mutated versions of this binding site (K233Q/R237Q/K251Q [KRK] or K325Q/K327Q [KK]) induced a significant delay of β-arrestin 2 recruitment (Fig. 5*B*) (3, 44). At the same time, the recovery of PI(4,5)P_2 was significantly retarded (Fig. 5*C*), suggesting that the PPI–arrestin interaction promotes PI(4,5)P_2 regeneration. Adaptor protein-2 (AP-2) also can interact directly with PIP5Ks and β-arrestins (47–49). Indeed, we found that barbadin, a blocker of the β-arrestin–AP-2 interaction (50), could reduce PI(4,5)P_2 regeneration. The actions of barbadin and of PPI binding-site mutations in arrestin were mutually occlusive since the reduction of regeneration by barbadin or by PPI binding-site mutantations of β-arrestin 2 were approximately similar to the reduction by the mutations combined with barbadin (Fig. 5*C*). The depletion of PI(4,5)P_2 was not fully saturated by these treatments as depletion of adenosine triphosphate (ATP) by oxygen scavengers caused more PI(4,5)P_2 reduction (Fig. 5C, blue dotted line). These experiments would be consistent with a functional interaction between β-arrestins and AP-2 during the PI(4,5)P_2 over recovery seen with long applications of AP.

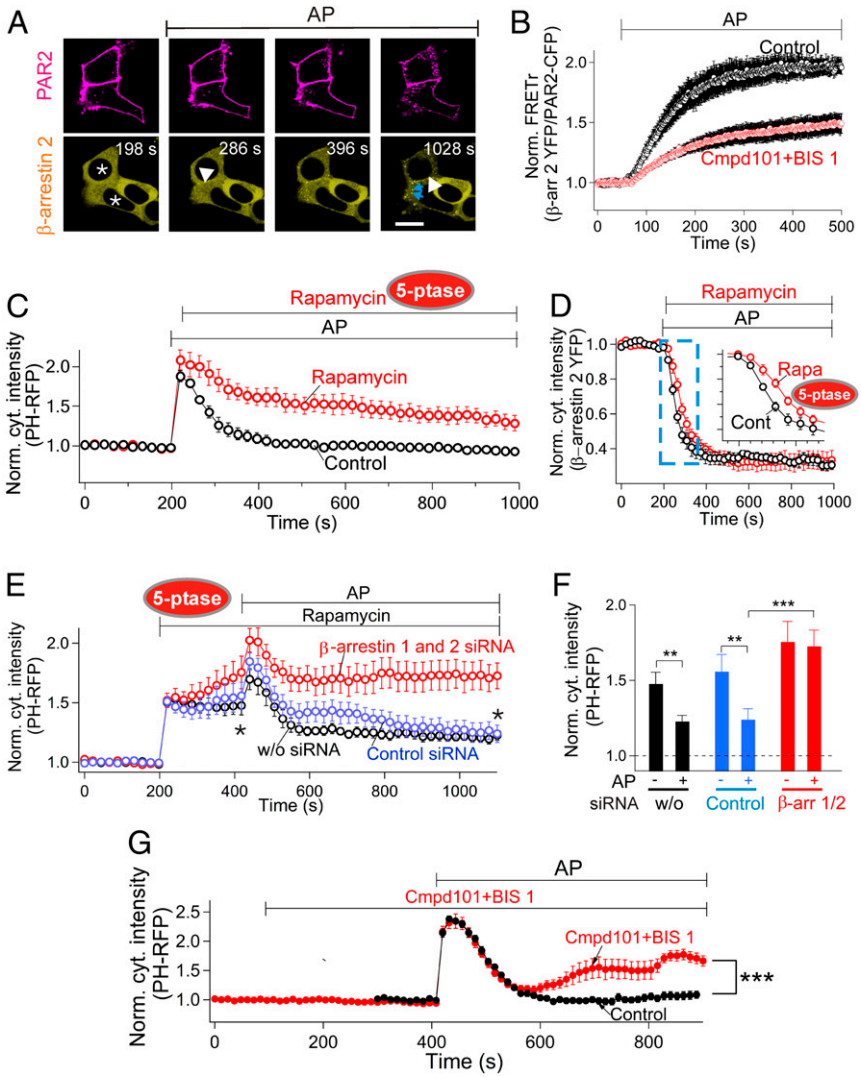

Fig. 3. β-arrestin boosts PI(4,5)P_2 synthesis at the PM. (*A*) Confocal images of translocation of β-arrestin-2-YFP to the PM during activation of PAR2. Cells were transiently transfected with dark-PAR2 labeled with an Alexa 647–conjugated primary antibody (magenta) and β-arrestin-2-YFP (yellow). The asterisks mark the nuclei of two cells expressing both the receptor and β-arrestin 2. (Scale bar, 10 μm.) The white arrowheads indicate PM-localized β-arrestin-2-YFP after AP treatment. The blue arrows indicate β-arrestin-2-YFP localized internalized receptors. (*B*) FRET between PAR2-CFP and β-arrestin-2-YFP showing direct interaction of β-arrestin 2 with activated PAR2 ($n = 6$ cells for control and $n = 7$ cells for cmpd101 + BIS1). (*C*) Time courses of cytoplasmic intensity of PH-RFP comparing control ($n = 8$ cells) and rapamycin-treated cells ($n = 6$ cells) where rapamycin recruited a 5-phosphatase to the PM to deplete PI(4,5)P_2. (*D*) Loss of cytoplasmic β-arrestin-2-YFP triggered by 100 μM AP with ($n = 6$ cells) or without ($n = 8$ cells) rapamycin. Rapamycin was applied right after AP to deplete PM PI(4,5)P_2 irreversibly. A decrease of β-arrestin-2-YFP in the cytoplasm indicates translocation of β-arrestin 2 to PAR2 at the PM. The blue-dashed area was enlarged as an inset. (*E*) Effect of β-arrestin 1 and 2 siRNA on recovery of PM PI(4,5)P_2 compared to with control siRNA or without siRNA. After partial depletion of PM PI(4,5)P_2 by rapamycin-recruited 5-phosphatase, PAR2 agonist (AP, 100 μM) was applied in the continued presence of rapamycin. Without siRNA ($n = 6$ cells), control siRNA ($n = 9$ cells), and β-arrestin 1 and 2 siRNA ($n = 8$ cells). (*F*) Mean cytoplasmic PH-RFP from the experiments in *E* measured at points marked by the two asterisks from before and after AP. (*G*) Effect of PKC and GRK2/3 blockers on PI(4,5)P_2 recovery ($n = 6$ cells for control and $n = 10$ cells for cmpd101 + BIS1). $^{**}P < 0.01$; $^{***}P < 0.005$.

We next looked at CCPs at the PM, structures critical for receptor endocytosis, using TIRF microscopy. After AP application, the total clathrin intensity of CCPs monitored in individual control cells showed an initial fall that soon reversed and even overshot above its starting level (Fig. 5*D*, control; *SI Appendix*, Fig. S7*A*). During this growth period, the mean lifetime of individual CCPs was 19% longer (64 ± 3 s, $n = 441$ events) than before AP treatment (54 ± 4 s, $n = 241$ events, $P = 0.03$; *SI Appendix*, Fig. S7*B*) as previously demonstrated (51, 52). The rate of formation of new CCPs was also increased by 12% (382 events per 210 s with AP versus 341 events per 210 s without AP). However, the intensity of single CCPs was not changed (538 ± 20 with AP versus 537 ± 22 without AP, *SI Appendix*, Fig. S7*C*). How about PI(4,5)P_2 dependency? The formation of CCPs upon PAR2 activation was attenuated by recruiting the 5-phosphatase to the PM (Fig. 5*D*, rapamycin). Because the mutants of β-arrestin 2 could reduce PI(4,5)P_2 regeneration, we also tested whether these mutants could inhibit formation of CCPs. Indeed, the KRK and the KK mutant of β-arrestin 2 significantly reduced CCP formation (Fig. 5*E*). Hence, we suggest that CCP formation is promoted by β-arrestin–dependent PI(4,5)P_2 regeneration.

What is the relationship of PAR2 endocytosis to β-arrestin? As shown in Fig. 5*F*, overexpression of wild-type (WT) β-arrestin 2 (open bar) significantly increased PAR2 endocytosis compared

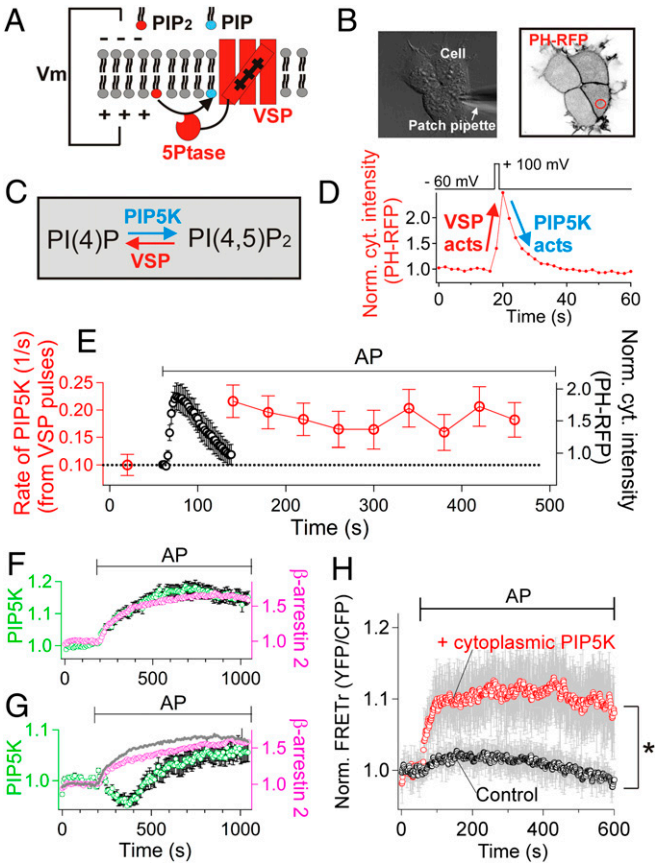

Fig. 4. PAR2 activates PIP5K. (*A*) Cartoon of voltage-sensitive 5-phosphatase (VSP) used to deplete PM PI(4,5)P_2. (*B*) Differential interference contrast (DIC) and confocal imaging combined with patch clamp. PAR2-CFP, GFP-VSP and PH-RFP were expressed at the same time. (*C*) Reaction scheme for PM PI(4,5)P_2 depletion by VSP and resynthesis by PIP5K. (*D*) Time course of cytoplasmic PH-RFP during and after one brief activation of VSP by a voltage jump. A representative trace. (*E*) Red symbols: Catalytic rate constant of PIP5K determined from the exponential recovery of PI(4,5)P_2 after repeated VSP pulses applied before and during treatment with AP (100 μM). Mean of five independent experiments. Black symbols: mean time course of PH-RFP probe translocation during the activation of PAR2 by AP. (*F* and *G*) Average intensity of clustered β-arrestin-2-mRFP and of GFP-PIP5K-Iγ recorded in conventional TIRF microscopy while AP was applied to PAR2-expressing cells. In the analysis, regions of interest (ROIs) containing individual β-arrestin-2-mRFP clusters (magenta) were selected to measure intensity changes of GFP-PIP5K-Iγ (green), reflecting recruitment of the kinase into β-arrestin 2 clusters. (*F*) One subset of data with monotonic PIP5K-Iγ recruitment into β-arrestin 2 clusters (group 1, 14 ROIs). (*G*) The second, remaining subset of data with biphasic PIP5K-Iγ signals at β-arrestin 2 clusters (group 2, 13 ROIs). The gray line was copied from the β-arrestin 2 clustering in *F* for comparison. The gray line and magenta symbols are significantly different ($P < 0.001$). (*H*) FRET between CFP-tagged cytoplasmic PIP5K-Iγ and YFP-tagged β-arrestin 2 ("+ cytoplasmic PIP5K," $n = 9$ cells). For the control experiments ("Control," $n = 8$ cells), cells were transfected with CFP instead of CFP-PIP5K-Iγ together with β-arrestin-2-YFP and dark PAR2. AP (100 μM) was used to activate PAR2 receptors. *$P < 0.05$.

to AP alone (gray bar), whereas the β-arrestin 2 mutants in the PI(4,5)P_2 binding site attenuated endocytosis (Fig. 5*F*, KRK (magenta) or KK alone (green)). Similarly, barbadin alone blocked PAR2 endocytosis (*SI Appendix*, Fig. S8), consistent with PI(4,5)P_2 dependence, and again, barbadin did not further potentiate the inhibitory effect when combined with the β-arrestin 2 mutants (Fig. 5*F*, KRK+barbadin (magenta) or KK+barbadin (green)). In sum, as receptors were desensitizing, receptor/β-arrestin/AP-2/PIP5K complexes formed, PIP5K was speeded, PI(4,5)P_2 production was augmented, more clathrin was recruited, CCPs were newly formed, and capture of desensitized receptors was potentiated for PI(4,5)P_2-dependent endocytosis of the complexes.

Active PAR2 Has Prolonged Interactions with CCPs. We turn now to the single-molecule level. Based on line-scan analysis of TIRF images, PAR2 receptors seemed strongly coclustered with CCPs (*SI Appendix*, Fig. S9). Single-molecule tracking revealed the stability of these putative complexes. A previous particle-tracking study of potassium channels being captured by forming CCPs showed transient interactions with dwell times shorter than the lifetime of a CCP (53); however, our impression was that β-arrestin/receptor complexes bound to CCPs more stably. We distinguished two contrasting modes of interaction with CCPs as the "immersion model" and the "boundary model" in Fig. 6*A* (*SI Appendix*, Fig. S10 for validation of single-molecule tracking). We followed the interaction using sparsely expressed PAR2s and CCPs in live cells. Before AP treatment, the PAR2 receptor molecules skirted around the CCPs making only transient interactions (*SI Appendix*, Fig. S11*A*). The mean dwell time was 0.9 ± 0.2 s, $n = 16$ receptors (Fig. 6*C* open symbols). However, after AP treatment and desensitization, the receptors developed prolonged interactions both with the edge of preexisting CCPs (Fig. 6*B* and *SI Appendix*, Figs. S11 *B* and *C* and S12) and with newly forming CCPs (*SI Appendix*, Figs. S11*D* and S12). The dwell time was increased almost 100-fold by AP application, 87 ± 13 s ($n = 31$ receptors, $P < 0.001$, Fig. 6*C*, red symbols).

If PAR2 receptors interacted with the edge of CCPs, we could estimate effective CCP dimensions from the center-to-center distance of the two fluorophores (Fig. 6*D* and *SI Appendix*, Fig. S13 for detailed analysis). The average diameter of CCPs was 124 nm, consistent with reported CCP diameters (9, 54). Direct STORM (dSTORM) imaging allowed us to visualize the geometry of β-arrestin clusters at the PM. Before super-resolution imaging, we confirmed that nearly all CCPs became clustered with β-arrestin 2 (Fig. 6*E*) as well as with PAR2 receptors (*SI Appendix*, Fig. S9). From the single-molecule tracking results, we had anticipated that β-arrestin stably bound to the receptor might gather in a ring encircling each CCP. In fact, the super-resolution images of β-arrestin 2 clusters revealed two spatial arrangements (Fig. 6*F*): 50% were the anticipated donut-shaped hollow structures (Fig. 6*G*) and 50% were fully filled ones (Fig. 6*H*). The former donut shape might represent β-arrestin–receptor complexes stably bound around the edge of preexisting CCPs as seen in the single-particle tracking (Fig. 6*B*), and the latter (filled-in structure) might represent newly forming CCPs incorporating β-arrestin–receptor complexes into them as they grew. Within our resolution limit, the estimated size of β-arrestin clusters in both cases was ~100 nm (Fig. 6 *G* and *H*), in accord with CCP sizes (Fig. 6*D*). To confirm whether CCPs can be a platform for β-arrestin–dependent PIP5K activation, we reduced CCP formation using Pitstop2 and clathrin heavy chain siRNA (*SI Appendix*, Fig. S14) and then measured PI(4,5)P_2 recovery. These conditions attenuated PI(4,5)P_2 regeneration significantly (Fig. 6*I*), suggesting that acceleration of PIP5Ks required β-arrestin–receptor clusters complexed with CCPs.

PIP5K-Iγ Binds Transiently with the PAR2/β-Arrestin/CCP Complex. Finally, we found that PIP5K-Iγ enzyme molecules were mobile (*SI Appendix*, Fig. S15) and that their apparent diffusion coefficient (0.65 ± 0.12 $\mu m^2/s$ in control, $n = 110$ molecules) was reduced by PAR2 activation (0.38 ± 0.06 $\mu m^2/s$, $n = 238$ molecules, $P < 0.05$). Our experiments suggested that this slowing might be attributed to transient interactions of PIP5K-Iγ with β-arrestin clustered at the CCPs. As shown in *SI Appendix*, Figs. S16 *A* and *B* and S18, density mapping of PIP5K-Iγs at the single-molecule level showed that the kinases began to linger around or within CCPs after PAR2 activation. Nearest neighbor distance analysis supported the idea that

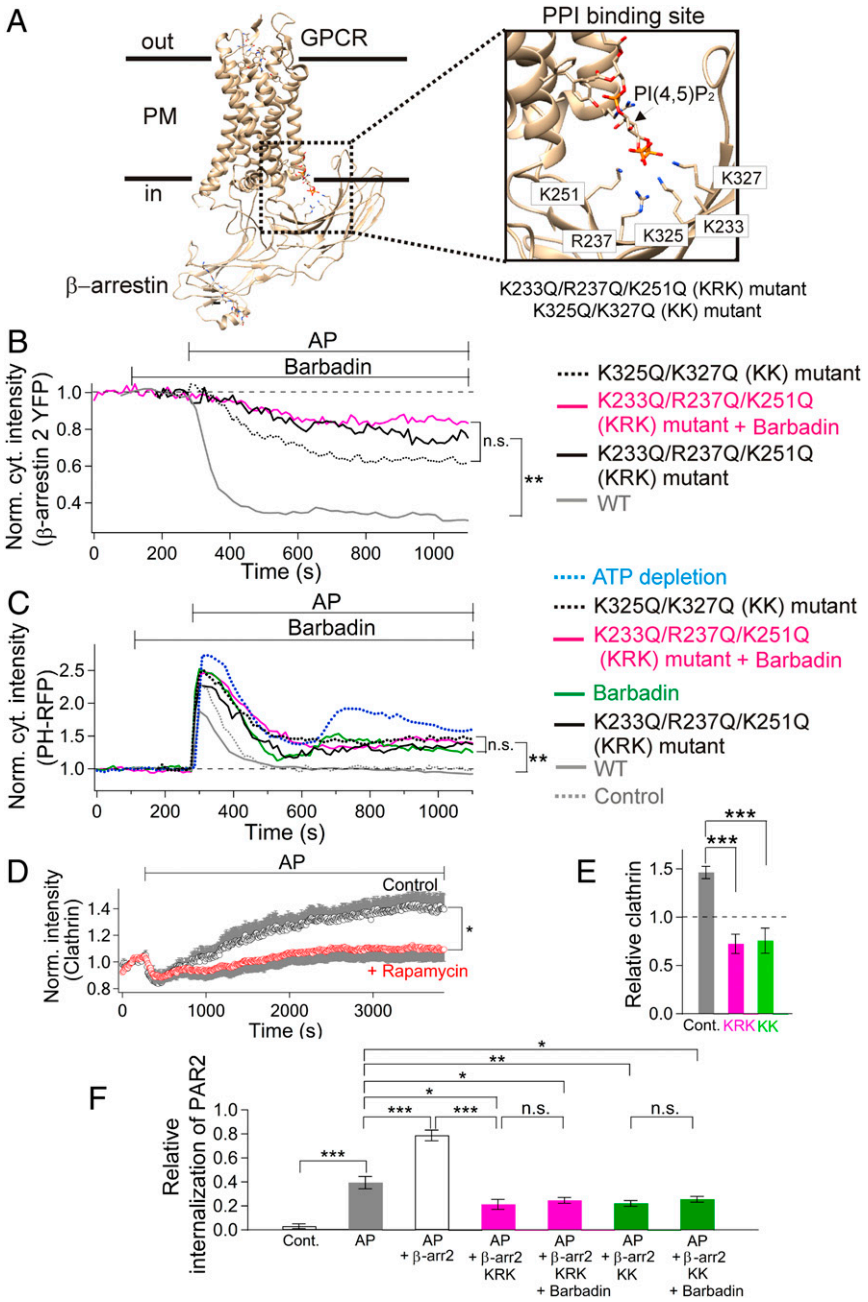

Fig. 5. The phosphoinositide binding site in β-arrestin controls PI(4,5)P_2 regeneration, CCPs, and PAR2 endocytosis. (*A*) Structure of neurotensin receptor 1 bound to β-arrestin 1 and PI(4,5)P_2 (PDB number: 6UP7, ref. 3). (*Inset*) Expanded image of the PPI binding site of β-arrestin 1. The K231, R235, K249, K323, and K325 residues of the β-arrestin 1 structure correspond to K233, R237, K251, K325, and K327 in β-arrestin 2. Phosphate oxygens of the PI(4,5)P_2 interact electrostatically with the positively charged polybasic residues in the PPI binding site. (*B*) Time course of β-arrestin-2-YFP translocation from the cytoplasm during AP. Translocation of WT β-arrestin-2-YFP and two mutant β-arrestins KRK or KK and occlusion of the barbadin effect. For the magenta trace, 50 μM barbadin was added 3 min before addition of 100 μM AP to the KRK mutant β-arrestin-2-YFP overexpressing cells (KRK mutant + barbadin, average cytoplasmic intensity between 800 and 1,000 s normalized to baseline: 0.83 ± 0.04, $n = 7$ cells). Also shown are traces with KRK (0.75 ± 0.08, $n = 5$ cells) and KK mutants alone (0.57 ± 0.02, $n = 6$ cells). The WT trace was from Fig. 3*D* (0.33 ± 0.02, $n = 8$ cells). (*C*) Reduction of late PI(4,5)P_2 recovery by overexpression of KRK or KK mutant β-arrestin 2. KRK mutant alone (average normalized cytoplasmic intensity between 800 and 1,000 s: 1.37 ± 0.11, $n = 6$ cells), KK mutant alone (1.47 ± 0.11, $n = 7$ cells), barbadin alone (1.38 ± 0.08, $n = 6$ cells), and KRK mutant + barbadin (1.39 ± 0.06, $n = 7$ cells). The PI(4,5)P_2 response after ATP reduction was added for comparison (1.87 ± 0.19, $n = 7$ cells). To reduce intracellular ATP in live cells, oxygen scavengers were added into the imaging chamber without additional metabolites (43). The WT trace was from Fig. 3*C* (0.92 ± 0.03, $n = 8$ cells). Control (no overexpression of β-arrestin-2-YFP, 1.01 ± 0.09, $n = 4$ cells). $^{**}P < 0.01$. n.s.: not significant. For the traces in *B* and *C*, error bars are omitted for better visibility. (*D*) Time course of formation of CCPs during AP and acute PM PI(4,5)P_2 depletion measured with TIRF. Total intensity of clathrin-DsRed from individual cells was measured. The intensity was normalized with before AP treatment and then averaged. Rapamycin was applied to recruit a 5-phosphatase soon after 100 μM AP ($n = 8$ cells, rapamycin), reducing the recovery of CCP formation as compared to the control ($n = 7$ cells). The error bars (in gray) are drawn on only one side of the data (circles) for clarity. (*E*) Statistics of relative clathrin-DsRed intensity at the PM (TIRF) after AP treatment for 60 min compared to the value before AP (dotted line). Control (no overexpression of β-arrestin-2-YFP, $n = 7$ cells), KRK mutant ($n = 9$ cells), or KK mutant ($n = 7$ cells) β-arrestin-2-YFP. $^{***}P < 0.001$. (*F*) Statistics of PAR2 endocytosis. Control (no drug treatment, $n = 17$ cells), AP ($n = 12$ cells), AP + WT β-arrestin-2-YFP ("β-arr 2," $n = 8$ cells), AP + KRK mutant β-arrestin-2-YFP ("β-arr 2 KRK," $n = 8$ cells), AP + KRK mutant β-arrestin-2-YFP + barbadin ("β-arr 2 KRK + Barbadin," $n = 15$ cells), AP + KK mutant β-arrestin-2-YFP ("β-arr 2 KK," $n = 28$ cells), and AP + KK mutant β-arrestin-2-YFP + barbadin ("β-arr 2 KK + Barbadin," $n = 30$ cells). $^{*}P < 0.05$; $^{**}P < 0.01$; $^{***}P < 0.005$.

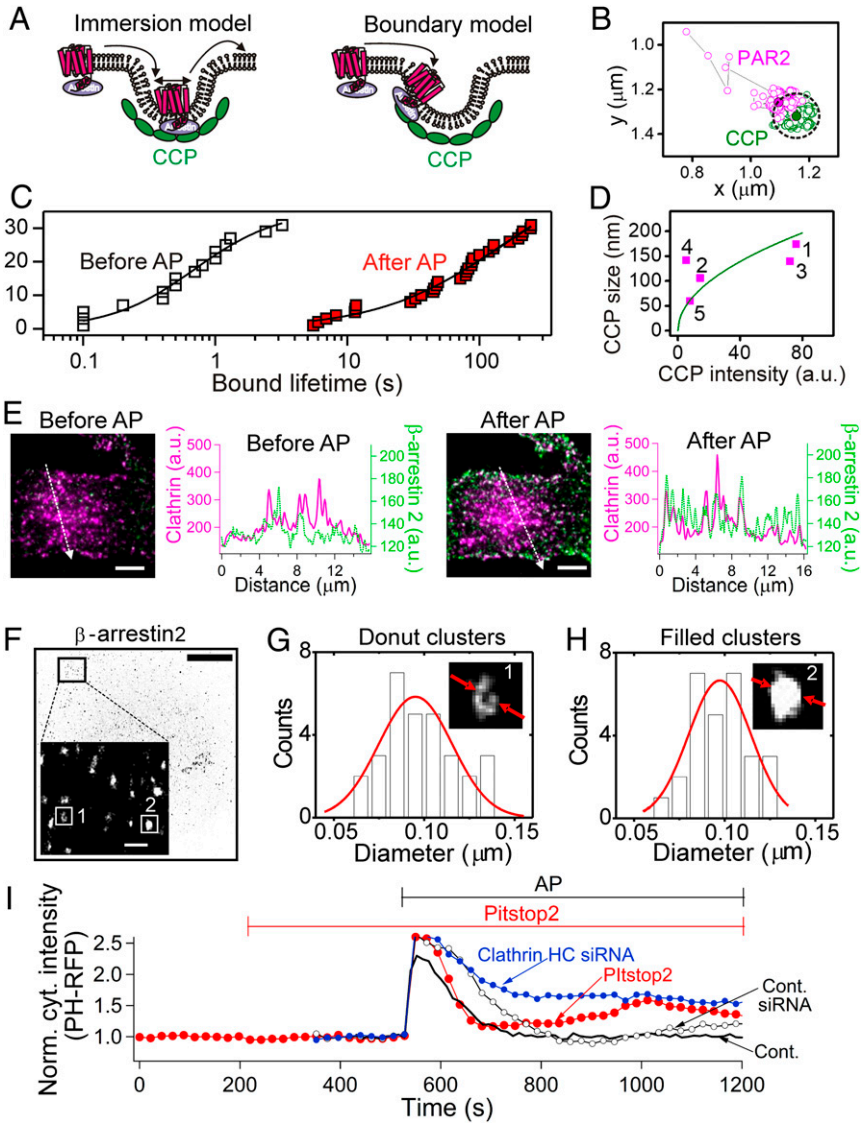

Fig. 6. Stable binding of PAR2/β-arrestin with CCP. (*A*) Two models for PAR2 interactions with CCPs: the immersion model and the boundary model. (*B–D*) Cells transiently transfected with PAR2 dark (~0.1 μg complementary DNA (cDNA)) and SNAP tagged clathrin light chain (~0.1 μg cDNA) studied by single-molecule live-cell imaging with TIRF microscopy (*SI Appendix, Methods and Materials*). (*B*) Representative single-molecule diffusion trajectory showing immobilization of one PAR2 molecule at a preexisting CCP. The dotted line indicates the effective boundary of CCP. (*C*) Cumulative distribution of bound lifetimes before (Mean: 0.9 ± 0.2 s, $n = 16$ events, open black symbol) and after AP treatment (87 ± 13 s, $n = 31$ events, red filled symbol). Data collected from three independent experiments. The bound lifetimes in each condition were plotted from smallest to largest values. (*D*) Summary of CCP size estimated by the center-to-center distance between the bound PAR2 receptors and CCPs versus CCP intensity. The green parabola plots the prediction that CCP size is proportional to (intensity of clathrin)$^{1/2}$. The average CCP size was 124 ± 14 nm ($n = 5$ cases from a single experiment, magenta). See *SI Appendix*, Fig. S13 for detailed information. (*E*) TIRF imaging showing recruitment of β-arrestin 2 to CCPs by PAR2 activation. Cells were transiently transfected with PAR2 dark (1 μg cDNA), β-arrestin-2-YFP (0.05 μg cDNA), and clathrin-DsRed (0.05 μg cDNA). TIRF images showing localization of β-arrestin 2 (green) and CCP (magenta) before and after AP addition. The line scans (white dotted line) showed only modest basal coclustering of β-arrestin 2 with CCP before addition of 100 μM AP and greater coclustering after AP. The image was taken ~10 min after addition of AP. (Scale bar, 4 μm.) (*F*) dSTORM image after endogenous β-arrestin 2 labeling with Alexa 647–conjugated primary antibodies. PAR2 was activated. (Scale bar, 5 μm.) Localization precision of Alexa 647 dyes and lateral resolution was 9 and 62 nm, respectively. (*Inset*) Expanded, noninverted fluorescence image to visualize the clustered β-arrestins. (Scale bar, 0.6 μm.) (*G*) Distribution of diameters of hollow structures from the difference of Gaussian peak positions. Mean: 98 ± 4 nm ($n = 30$ clusters). (*Inset*) One typical β-arrestin 2 donut cluster. (*H*) Distribution of diameters of high-density β-arrestin 2 clusters without hollow structure from full-width-at-half-maximum. Mean: 97 ± 4 nm ($n = 28$ clusters). (*Inset*) One typical filled β-arrestin 2 cluster. The data were collected from one representative result among six independent experiments. (*I*) Effects of blocking CCP formation on normalized cytoplasmic PH-RFP intensity during AP application. Average traces without error bars are shown for better visibility. Pitstop2 (average normalized cytoplasmic PH-RFP intensity between 1,000 and 1,200 s: 1.46 ± 0.13, $n = 6$ cells, $P < 0.05$) compared to control (1.0 ± 0.09, $n = 4$ cells) or clathrin heavy chain siRNA (average cytoplasmic PH-RFP intensity between 800 and 1,000 s: 1.65 ± 0.16, $n = 6$ cells, $P < 0.005$) compared to control siRNA (0.96 ± 0.1, $n = 4$ cells).

during PAR2 activation, PIP5K-Iγs stayed closer to the CCPs (*SI Appendix*, Figs. S16 *C* and *D* and S17). Similarly, we confirmed that PIP5K-Iγ could be localized with WT β-arrestin 2 clusters but not with the KRK mutant β-arrestin 2 (*SI Appendix*, Fig. S19), and that the mutant β-arrestins were also not clustered with CCPs (*SI Appendix*, Fig. S20). Evidently, without interactions with β-arrestin, PIP5K was less localized to CCPs and not potentiating PI(4,5)P_2 resynthesis or PAR2 endocytosis.

Discussion

We have presented a sequence of events diagrammed in Fig. 7: An activated PAR2 receptor couples to PLC and depletes the PM $PI(4,5)P_2$ pool. Then, the active receptors are desensitized by rapid phosphorylation, and β-arrestin binds to them. In turn, this complex can bind stably to CCPs forming a β-arrestin–receptor–CCP supercomplex that recruits PIP5Ks transiently to accelerate $PI(4,5)P_2$ resynthesis at the PM. The speeded resynthesis draws on precusor PI(4)P from both Golgi and PM pools. Finally, formation of β-arrestin–PIP5K complexes and augmented $PI(4,5)P_2$ at the CCPs accelerate new formation of CCPs and promote recruitment of $PI(4,5)P_2$-dependent endocytic machinery for final PAR2 internalization.

Transferrin receptors have been a model system to study clathrin-mediated receptor endocytosis. With that receptor, it is reported that the influence of the PM PI(4)P pool on receptor endocytosis is minimal as judged by depleting PI(4)P with PM-localizing Sac1 (55). However, in our work with PAR2, PPIs seem to play a more pervasive role. Receptor activation was followed by a β-arrestin–induced acceleration of PIP5K that speeded resynthesis of PM $PI(4,5)P_2$ and promoted CCP formation. In our experiments, targeted depletion of PI(4)P pools reduced both PM $PI(4,5)P_2$ and internalization of PAR2. It seems possible that endocytosis of transferrin receptor also could be modulated by β-arrestin–dependent $PI(4,5)P_2$ regeneration, a hypothesis that needs testing in the future.

In agreement with Ricks and Trejo (8), our results support the canonical β-arrestin–, clathrin- and dynamin-dependent internalization of PAR2 recognized for other GPCRs (4, 6, 7, 9). We found that desensitized PAR2 receptors became effectively immobilized at CCPs possibly reflecting a local increase of $PI(4,5)P_2$ there and a stimulated accumulation of adaptor proteins, clathrin, and dynamin. Dynamin mediates the final fission of clathrin-coated vesicles (10, 12, 56). Cryo-EM structures of β-arrestin–GPCR complexes show $PI(4,5)P_2$ as an auxiliary component of stable complexes (3). Similarly, protein mass spectrometry has provided insights for regulation of G protein selection by membrane PPIs, especially $PI(4,5)P_2$ (2). We found that the rate of β-arrestin recruitment was slower when $PI(4,5)P_2$ was depleted at the PM, yet we also observed that the final extent of recruitment was not much changed, consistent with previous reports (45). Apparently, even when $PI(4,5)P_2$ is low, β-arrestin in the complex eventually interacts adequately with the membrane (57) and with other signaling molecules such as ERK/MAPK (58) and, in this study, PIP5K.

We now turn to speculative interpretations. It has been proposed that β-arrestin has a direct interaction with PIP5K-Iα that requires the KRK region in the C domain of β-arrestin (46). We observed a modest twofold increase of PIP5K activity by β-arrestins and that the β-arrestin–receptor–CCP complex is strong and sustained. Perhaps transient binding of PIP5K to β-arrestin in this complex can induce allosteric modulation of PIP5K activity, effectively doubling the catalytic rate constant for $PI(4,5)P_2$ regeneration. CCPs may serve as a local platform for $PI(4,5)P_2$ regeneration as well as for capturing desensitized receptors and mediating endocytosis. AP-2 has direct binding sites for PIP5K (47–49), β-arrestin (50, 59), and clathrin (60) that may coordinate the β-arrestin–receptor–PIP5K–CCP interaction. Indeed, barbadin, a small molecule that blocks β-arrestin–AP-2 interactions, reduced $PI(4,5)P_2$ recovery and PAR2 endocytosis, an action occluded by PPI binding site mutants of β-arrestin. The reduction of $PI(4,5)P_2$ recovery would be consistent with the hypothesis that β-arrestin–AP-2 interactions in CCPs boost the local activity of PIP5K at the PM. In our study, the majority of overexpressed PIP5K-Iγ localized to the PM as previously demonstrated (47). This makes sense since a PM localization of 5-kinases would be critical to produce $PI(4,5)P_2$ uniquely at the PM and not at other intracellular compartments. If the PIP5Ks bound strongly to receptor/β-arrestin/AP2/CCP complexes, receptor endocytosis would promote intracellular trafficking of the kinases. Thus, the transient nature of PIP5K binding might reduce loss of PIP5Ks from the PM. More studies of the detailed kinetics of the interactions and conformational changes of these proteins and the actions of other subtypes of PIP5Ks are needed.

Are there contributions of other PPIs to receptor endocytosis? Another isoform of PIP_2, $PI(3,4)P_2$, and also PI(3)P, an endosomal PPI formed from $PI(3,4)P_2$, have been implicated in the last stages of endocytosis (61, 62). They recruit SNX9, a BAR-domain

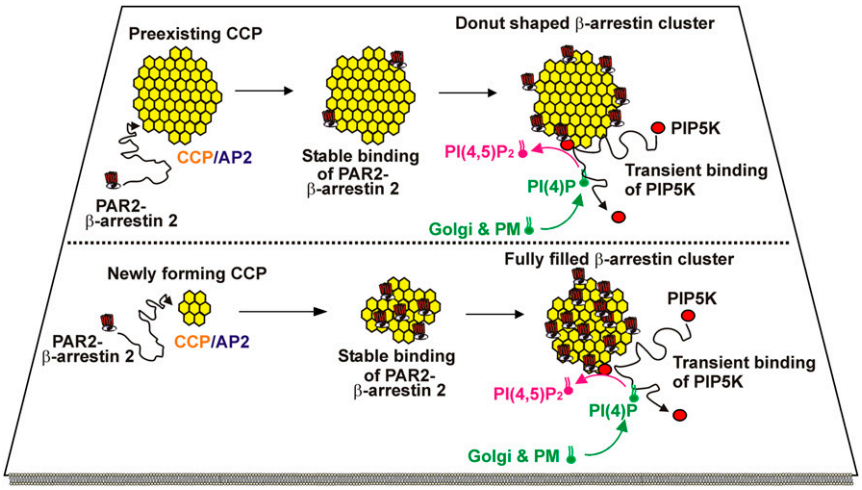

Fig. 7. Working hypothesis for β-arrestin–dependent PIP5K-Iγ recruitment and $PI(4,5)P_2$ regeneration at CCPs. CCPs are represented as a yellow hexagonal lattice with lattice spacing of 10 to 12 nm according to electron microscope images and super-resolution imaging (9, 54). Receptor–β-arrestin complexes join and interact tightly with the boundary of preexisting CCPs (*Upper*) or become incorporated more internally within newly forming CCPs (*Lower*). The preexisting CCPs vary in size, and the newly forming CCPs are growing in time. Therefore, snapshot images of those states would yield different sizes of β-arrestin clusters (as measured in Fig. 6 *D*, *F*, and *G*). Mobile PIP5K-Iγs bind transiently to receptor/β-arrestin/AP-2 complexes on CCPs. The complexed PIP5K-Iγs converts laterally diffusing PI(4)P to $PI(4,5)P_2$ locally at the CCPs (a twofold increase of activity), promoting $PI(4,5)P_2$-dependent endocytosis. Preexisting CCPs are shown as accumulating a donut-shaped peripheral ring of PAR2 receptor complexes forming a hollow structure. By comparison, newly forming CCPs grow continuously to make mature CCPs with β-arrestins dispersed within them (nonhollow structure). As CCPs grow with AP-2, more β-arrestin–PAR2 receptor complexes can accumulate into the growing structure. After maturation and depending on the amount of $PI(4,5)P_2$, the CCP may be internalized.

protein to form a highly curved membrane after the formation of clathrin-coated vesicles. About this proposal, another group suggested that conversion of $PI(4,5)P_2$ to $PI(3,4)P_2$ and PI(3)P is not likely until dynamin completes the scission of a CCP because lipid molecules would be exchanged rapidly between the PM and still-connected clathrin-coated vesicles (14). Thus, $PI(4,5)P_2$ may be the principal PPI participating in initiation of receptor endocytosis, as suggested by others (11, 55, 63).

Our analysis with PAR2 revealed roles of β-arrestin–dependent $PI(4,5)P_2$ regeneration in GPCR desensitization and endocytosis: 1) ligand-bound PAR2 upregulates the activity of PIP5-kinase at the PM twofold in a β-arrestin–dependent manner; 2) $PI(4,5)P_2$ accelerates receptor interactions with β-arrestin; 3) Golgi and PM pools of PI(4)P contribute to regeneration of PM $PI(4,5)P_2$ and to increase PAR2 endocytosis; 4) desensitized PAR2 receptors are immobilized on contact with CCPs and remain there ∼100 times longer than unactivated receptors; 5) β-arrestin–receptor complexes localize to the edge of already present CCPs and also are incorporated within CCPs as they are forming de novo; and 6) transient binding of PIP5K-Iγ to β-arrestin/receptor/CCP complexes can upregulate $PI(4,5)P_2$ regeneration near CCPs. Our findings emphasize the versatility of β-arrestin cooperating with several partners, regulating PPI pools, and inducing receptor endocytosis. Our study should help to understand PAR2- and $PI(4,5)P_2$-mediated cellular mechanisms related to human diseases including cancer metastasis, pain, and inflammation.

Materials and Methods

See *SI Appendix* for full description of the reagents and methods. Briefly, experiments were performed at room temperature on human embryonic kidney (HEK) cell–derived tsA201 cells transiently transfected with complementary DNA plasmids for PAR2 receptors, fluorescent markers for PI(4)P and $PI(4,5)P_2$, translocatable 4-phosphatase and 5-phosphatase enzymes, clathrin, normal and mutant β-arrestins, and siRNA against clathrin heavy chain or β-arrestins. Measurements were made on living cells with FRET photometry, confocal microscopy, conventional TIRF microscopy and single-molecule TIRF microscopy, and direct STORM imaging with fixed cells. Mean values are shown with SEM. Statistical significance was tested with Student's *t* test. If the *P* value was smaller than 0.05, the difference was considered significant (*, **, ***, and **** for $P < 0.05$, 0.01, 0.005, and 0.001, respectively).

Data Availability. All study data are included in the article and/or *SI Appendix*.

ACKNOWLEDGMENTS. We thank Lea M. Miller for technical assistance and Drs. Eamonn J. Dickson and Jill B. Jensen for discussion. We thank Drs. Oscar Vivas, Jill B. Jensen, Lizbeth de la Cruz, Jongyun Myeong, and Gucan Dai for their comments. Our work was supported by the National Research Foundation of Korea (NRF) grant funded by the Korea government (MSIT, NRF-2019R1A2C1005719 to J.B.S.) and NIH (R01-MH113333 to D.T.C., R01-DK080840 to D.S.K., and R01-GM083913 and R37-NS08174 to B.H.).

1. H. J. McCrea, P. De Camilli, Mutations in phosphoinositide metabolizing enzymes and human disease. 24:8-16. *Physiology (Bethesda)* **24**, 8–16 (2009).
2. H. Y. Yen *et al*., PtdIns(4,5)P_2 stabilizes active states of GPCRs and enhances selectivity of G-protein coupling. *Nature* **559**, 423–427 (2018).
3. W. Huang *et al*., Structure of the neurotensin receptor 1 in complex with β-arrestin 1. *Nature* **579**, 303–308 (2020).
4. Y. Posor, M. Eichhorn-Grünig, V. Haucke, Phosphoinositides in endocytosis. *Biochim. Biophys. Acta* **1851**, 794–804 (2015).
5. L. M. Luttrell, R. J. Lefkowitz, The role of beta-arrestins in the termination and transduction of G-protein-coupled receptor signals. *J. Cell Sci.* **115**, 455–465 (2002).
6. S. A. Laporte, R. H. Oakley, J. A. Holt, L. S. Barak, M. G. Caron, The interaction of β-arrestin with the AP-2 adaptor is required for the clustering of β 2-adrenergic receptor into clathrin-coated pits. *J. Biol. Chem.* **275**, 23120–23126 (2000).
7. F. Santini, I. Gaidarov, J. H. Keen, G protein-coupled receptor/arrestin3 modulation of the endocytic machinery. *J. Cell Biol.* **156**, 665–676 (2002).
8. T. K. Ricks, J. Trejo, Phosphorylation of protease-activated receptor-2 differentially regulates desensitization and internalization. *J. Biol. Chem.* **284**, 34444–34457 (2009).
9. K. A. Sochacki, A. M. Dickey, M. P. Strub, J. W. Taraska, Endocytic proteins are partitioned at the edge of the clathrin lattice in mammalian cells. *Nat. Cell Biol.* **19**, 352–361 (2017).
10. M. Rosendale *et al*., Functional recruitment of dynamin requires multimeric interactions for efficient endocytosis. *Nat. Commun.* **10**, 4462 (2019).
11. R. Zoncu *et al*., Loss of endocytic clathrin-coated pits upon acute depletion of phosphatidylinositol 4,5-bisphosphate. *Proc. Natl. Acad. Sci. U.S.A.* **104**, 3793–3798 (2007).
12. D. Loerke *et al*., Cargo and dynamin regulate clathrin-coated pit maturation. *PLoS Biol.* **7**, e57 (2009).
13. T. Kirchhausen, D. Owen, S. C. Harrison, Molecular structure, function, and dynamics of clathrin-mediated membrane traffic. *Cold Spring Harb. Perspect. Biol.* **6**, a016725 (2014).
14. K. He *et al*., Dynamics of phosphoinositide conversion in clathrin-mediated endocytic traffic. *Nature* **552**, 410–414 (2017).
15. M. G. Roth, Phosphoinositides in constitutive membrane traffic. *Physiol. Rev.* **84**, 699–730 (2004).
16. I. van den Bout, N. Divecha, PIP5K-driven PtdIns(4,5)P_2 synthesis: regulation and cellular functions. *J. Cell Sci.* **122**, 3837–3850 (2009).
17. T. Balla, Phosphoinositides: Tiny lipids with giant impact on cell regulation. *Physiol. Rev.* **93**, 1019–1137 (2013).
18. Y. J. Kim, M. L. Guzman-Hernandez, E. Wisniewski, T. Balla, Phosphatidylinositol-phosphatidic acid exchange by Nir2 at ER-PM contact sites maintains phosphoinositide signaling competence. *Dev. Cell* **33**, 549–561 (2015).
19. E. J. Dickson *et al*., Dynamic formation of ER-PM junctions presents a lipid phosphatase to regulate phosphoinositides. *J. Cell Biol.* **213**, 33–48 (2016).
20. C. J. Stefan *et al*., Osh proteins regulate phosphoinositide metabolism at ER-plasma membrane contact sites. *Cell* **144**, 389–401 (2011).
21. C. J. Stefan *et al*., Membrane dynamics and organelle biogenesis-lipid pipelines and vesicular carriers. *BMC Biol.* **15**, 102 (2017).
22. M. Sohn *et al*., $PI(4,5)P_2$ controls plasma membrane PI4P and PS levels via ORP5/8 recruitment to ER-PM contact sites. *J. Cell Biol.* **217**, 1797–1813 (2018).
23. B. Mesmin, D. Kovacs, G. D'Angelo, Lipid exchange and signaling at ER-Golgi contact sites. *Curr. Opin. Cell Biol.* **57**, 8–15 (2019).
24. E. J. Dickson, J. B. Jensen, B. Hille, Golgi and plasma membrane pools of PI(4)P contribute to plasma membrane $PI(4,5)P_2$ and maintenance of KCNQ2/3 ion channel current. *Proc. Natl. Acad. Sci. U.S.A.* **111**, E2281–E2290 (2014).
25. G. B. Willars, S. R. Nahorski, R. A. Challiss, Differential regulation of muscarinic acetylcholine receptor-sensitive polyphosphoinositide pools and consequences for signaling in human neuroblastoma cells. *J. Biol. Chem.* **273**, 5037–5046 (1998).
26. L. F. Horowitz *et al*., Phospholipase C in living cells: Activation, inhibition, Ca^{2+} requirement, and regulation of M current. *J. Gen. Physiol.* **126**, 243–262 (2005).
27. A. Balla *et al*., Maintenance of hormone-sensitive phosphoinositide pools in the plasma membrane requires phosphatidylinositol 4-kinase IIIalpha. *Mol. Biol. Cell* **19**, 711–721 (2008).
28. Z. Szentpetery, P. Várnai, T. Balla, Acute manipulation of Golgi phosphoinositides to assess their importance in cellular trafficking and signaling. *Proc. Natl. Acad. Sci. U.S.A.* **107**, 8225–8230 (2010).
29. R. Ramachandran, C. Altier, K. Oikonomopoulou, M. D. Hollenberg, Proteinases, their extracellular targets, and inflammatory signaling. *Pharmacol. Rev.* **68**, 1110–1142 (2016).
30. Y. Dai *et al*., Proteinase-activated receptor 2-mediated potentiation of transient receptor potential vanilloid subfamily 1 activity reveals a mechanism for proteinase-induced inflammatory pain. *J. Neurosci.* **24**, 4293–4299 (2004).
31. L. Yang *et al*., Proteinase-activated receptor 2 promotes cancer cell migration through RNA methylation-mediated repression of miR-125b. *J. Biol. Chem.* **290**, 26627–26637 (2015).
32. R. Ramachandran, F. Noorbakhsh, K. Defea, M. D. Hollenberg, Targeting proteinase-activated receptors: Therapeutic potential and challenges. *Nat. Rev. Drug Discov.* **11**, 69–86 (2012).
33. R. K. Y. Cheng *et al*., Structural insight into allosteric modulation of protease-activated receptor 2. *Nature* **545**, 112–115 (2017).
34. V. S. Ossovskaya, N. W. Bunnett, Protease-activated receptors: Contribution to physiology and disease. *Physiol. Rev.* **84**, 579–621 (2004).
35. M. H. Kim *et al*., Protease-activated receptor-2 increases exocytosis via multiple signal transduction pathways in pancreatic duct epithelial cells. *J. Biol. Chem.* **283**, 18711–18720 (2008).
36. A. K. S. Arakaki, W.-A. Pan, J. Trejo, GPCRs in Cancer: Protease-activated receptors, endocytic adaptors and signaling. *Int. J. Mol. Sci.* **19**, E1886 (2018).
37. P. Zhao, M. Metcalf, N. W. Bunnett, Biased signaling of protease-activated receptors. *Front. Endocrinol. (Lausanne)* **5**, 67 (2014).
38. S. R. Jung *et al*., Contributions of protein kinases and β-arrestin to termination of protease-activated receptor 2 signaling. *J. Gen. Physiol.* **147**, 255–271 (2016).
39. E. Brombacher *et al*., Rab1 guanine nucleotide exchange factor SidM is a major phosphatidylinositol 4-phosphate-binding effector protein of Legionella pneumophila. *J. Biol. Chem.* **284**, 4846–4856 (2009).
40. G. R. Hammond, M. P. Machner, T. Balla, A novel probe for phosphatidylinositol 4-phosphate reveals multiple pools beyond the Golgi. *J. Cell Biol.* **205**, 113–126 (2014).
41. B. C. Suh, T. Inoue, T. Meyer, B. Hille, Rapid chemically induced changes of PtdIns(4,5)P_2 gate KCNQ ion channels. *Science* **314**, 1454–1457 (2006).
42. H. M. Rohde *et al*., The human phosphatidylinositol phosphatase SAC1 interacts with the coatomer I complex. *J. Biol. Chem.* **278**, 52689–52699 (2003).
43. S. R. Jung *et al*., Minimizing ATP depletion by oxygen scavengers for single-molecule fluorescence imaging in live cells. *Proc. Natl. Acad. Sci. U.S.A.* **115**, E5706–E5715 (2018).
44. K. Eichel *et al*., Catalytic activation of β-arrestin by GPCRs. *Nature* **557**, 381–386 (2018).
45. D. J. Tóth *et al*., Acute depletion of plasma membrane phosphatidylinositol 4,5-bisphosphate impairs specific steps in endocytosis of the G-protein-coupled receptor. *J. Cell Sci.* **125**, 2185–2197 (2012).

46. C. D. Nelson, J. J. Kovacs, K. N. Nobles, E. J. Whalen, R. J. Lefkowitz, β-arrestin scaffolding of phosphatidylinositol 4-phosphate 5-kinase Ialpha promotes agonist-stimulated sequestration of the β2-adrenergic receptor. *J. Biol. Chem.* **283**, 21093–21101 (2008).
47. M. Krauss, V. Kukhtina, A. Pechstein, V. Haucke, Stimulation of phosphatidylinositol kinase type I-mediated phosphatidylinositol (4,5)-bisphosphate synthesis by AP-2μ-cargo complexes. *Proc. Natl. Acad. Sci. U.S.A.* **103**, 11934–11939 (2006).
48. J. R. Thieman *et al*., Clathrin regulates the association of PIPKIγ661 with the AP-2 adaptor β2 appendage. *J. Biol. Chem.* **284**, 13924–13939 (2009).
49. N. Kahlfeldt *et al*., Molecular basis for association of PIPKIγ-p90 with clathrin adaptor AP-2. *J. Biol. Chem.* **285**, 2734–2749 (2010).
50. A. Beautrait *et al*., A new inhibitor of the β-arrestin/AP2 endocytic complex reveals interplay between GPCR internalization and signalling. *Nat. Commun.* **8**, 15054 (2017).
51. M. A. Puthenveedu, M. von Zastrow, Cargo regulates clathrin-coated pit dynamics. *Cell* **127**, 113–124 (2006).
52. M. Lampe, F. Pierre, S. Al-Sabah, C. Krasel, C. J. Merrifield, Dual single-scission event analysis of constitutive transferrin receptor (TfR) endocytosis and ligand-triggered B2-adrenergic receptor (B2AR) or Mu-opioid receptor (MOR) endocytosis. *Mol. Biol. Cell* **25**, 3070–3080 (2014).
53. A. V. Weigel, M. M. Tamkun, D. Krapf, Quantifying the dynamic interactions between a clathrin-coated pit and cargo molecules. *Proc. Natl. Acad. Sci. U.S.A.* **110**, E4591–E4600 (2013).
54. N. M. Willy *et al*., Endocytic clathrin coats develop curvature at early stages of their formation. *bioRxiv* [Preprint] (2019). https://doi.org/10.1101/715219 (Accessed 26 July 2019).
55. G. R. Hammond *et al*., PI4P and PI(4,5)P2 are essential but independent lipid determinants of membrane identity. *Science* **337**, 727–730 (2012).
56. M. Mettlen, T. Pucadyil, R. Ramachandran, S. L. Schmid, Dissecting dynamin's role in clathrin-mediated endocytosis. *Biochem. Soc. Trans.* **37**, 1022–1026 (2009).
57. D. P. Staus *et al*., Structure of the M2 muscarinic receptor-β-arrestin complex in a lipid nanodisc. *Nature* **579**, 297–302 (2020).
58. S. R. Jung, C. Kushmerick, J. B. Seo, D. S. Koh, B. Hille, Muscarinic receptor regulates extracellular signal regulated kinase by two modes of arrestin binding. *Proc. Natl. Acad. Sci. U.S.A.* **114**, E5579–E5588 (2017).
59. S. Chakraborty *et al*., A phosphotyrosine switch for cargo sequestration at clathrin-coated buds. *J. Biol. Chem.* **289**, 17497–17514 (2014).
60. O. Kovtun, V. K. Dickson, B. T. Kelly, D. J. Owen, J. A. G. Briggs, Architecture of the AP2/clathrin coat on the membranes of clathrin-coated vesicles. *Sci. Adv.* **6**, eaba8381 (2020).
61. Y. Posor *et al*., Spatiotemporal control of endocytosis by phosphatidylinositol-3,4-bisphosphate. *Nature* **499**, 233–237 (2013).
62. S. L. Schmid, M. Mettlen, Cell biology: Lipid switches and traffic control. *Nature* **499**, 161–162 (2013).
63. W. Yamamoto *et al*., Distinct roles for plasma membrane PtdIns(4)P and PtdIns(4,5)P_2 during receptor-mediated endocytosis in yeast. *J. Cell Sci.* **131**, jcs207696 (2018).